Kinetic Mechanism of Quinone Oxidoreductase 2 and Its Inhibition by the Antimalarial Quinolines†

Jesse J. Kwiek,[§,⊥] Timothy A. J. Haystead,[§,||] and Johannes Rudolph*[,#]

Department of Pharmacology and Cancer Biology, Department of Biochemistry, Box 3813, Research Drive, Duke University, Durham, North Carolina 27710, and Serenex, Inc., Durham, North Carolina 27701

Received October 28, 2003; Revised Manuscript Received February 4, 2004

ABSTRACT: Quinone oxidoreductase 2 (QR2) purified from human red blood cells was recently shown to be a potential target of the quinoline antimalarial compounds [Graves et al., (2002) *Mol. Pharmacol. 62*, 1364]. QR2 catalyzes the two-electron reduction of menadione via the oxidation of *N*-alkylated or *N*-ribosylated nicotinamides. To investigate the mechanism and consequences of inhibition of QR2 by the quinolines further, we have used steady-state and transient-state kinetics to define the mechanism of QR2. Importantly, we have shown that QR2 when isolated from an overproducing strain of *E. coli* is kinetically equivalent to the enzyme from the native human red blood cell source. We observe ping-pong kinetics consistent with one substrate/inhibitor binding site that shows selectivity for the oxidation state of the FAD cofactor, suggesting that selective inhibition of the liver versus red blood cell forms of malaria may be possible. The reductant *N*-methyldihydronicotinamide and the inhibitor primaquine bind exclusively to the oxidized enzyme. In contrast, the inhibitors quinacrine and chloroquine bind exclusively to the reduced enzyme. The quinone substrate menadione, on the other hand, binds nonspecifically to both forms of the enzyme. Single-turnover kinetics of the reductive half-reaction are chemically and kinetically competent and confirm the inhibitor selectivity seen in the steady-state experiments. Our studies shed light on the possible in vivo potency of the quinolines and provide a foundation for future studies aimed at creating more potent QR2 inhibitors and at understanding the physiological significance of QR2.

Human quinone oxidoreductase 2 (QR2)[1] was first isolated in 1961 as a widely distributed cytosolic flavoenzyme that catalyzed the oxidation of nonphosphorylated dihydronicotinamides such as *N*-methyldihydronicotinamide (NMeH) or *N*-ribosyldihydronicotinamide (*1*). QR2 stood in contrast to QR1 (also known as DT-diaphorase) that preferred the phosphorylated dihydronicotinamides such as NADH and NADPH (*2*). QR1 is proposed to perform three physiological roles. It catalyzes the reduction of vitamin K, while contributing to the synthesis of blood coagulation cofactors in hepatocytes, protects cells against oxidative stress by transforming quinones into hydroquinones, and activates antitumor prodrugs such as the mitomycins, anthracydins, and aziridinylbenzoquinones (*3*−*5*). Whereas QR1 has been extensively studied for these physiological roles, QR2 became the "long-forgotten flavoenzyme". It was not until 1997 that QR2 was biochemically rediscovered as the product of the $hNQO_2$ gene (*6*), identified 7 years earlier in a screen of a cDNA library with a QR1 probe in an attempt to purify novel QR1 enzymes (*7*). Amino acid sequence alignment of QR1 and QR2 indicates 49% sequence identity, with the major difference being the lack of a 43-residue C-terminal tail in QR2. The crystal structures of QR1 (*8*) and QR2 (*9*) are highly similar, both forming homodimers with two independent and equivalent active sites each containing a FAD cofactor. Interestingly, the C-terminal tail that is absent in QR2 was shown to be important for binding the ADP moiety of NAD(P)H in the crystal structure of QR1, thus explaining the lack of reactivity of NAD(P)H with QR2.

The mechanism and reactivity of QR1 (EC 1.6.99.2) have been extensively characterized (*10*, *11*). Consistent with the crystal structure showing that NAD(P)H and the substrate bind in overlapping sites, the enzyme utilizes a ping-pong mechanism. This is more reminiscent of electron carriers such as flavodoxin and less similar to typical oxidoreductases that can bind nicotinamides and substrates simultaneously. The enzyme is very fast, having second-order rate constants with NADPH at $\sim 1 \times 10^9$ M^{-1} s^{-1} with no saturating behavior toward nicotinamides. The lack of an enzyme−substrate complex with a significant lifetime is consistent with a weak affinity for substrates and its broad substrate specificity. QR1 is potently inhibited by dicoumerol, a competitive inhibitor, versus NAD(P)H (*12*). Rapid reaction kinetics with QR1 are monophasic with no evidence for a stepwise one-electron mechanism or transient formation of a semiquinoid inter-

† This work was partially funded by a new initiative in malaria research award (to T.A.J.H.) from the Burroughs Wellcome Fund.

* To whom correspondence should be addressed. Tel: 919-668-6188. Fax: 919-613-8642. E-mail: rudolph@biochem.duke.edu.

§ Department of Pharmacology and Cancer Biology.

⊥ Current address: Department of Microbiology and Immunology, CB 7290, UNC−Chapel Hill, NC 27599.

|| Serenex, Inc.

Department of Biochemistry.

[1] Abbreviations: QR1, quinone oxidoreductase 1; QR2, quinone oxidoreductase 2; $QR2_{nat}$, QR2 derived from red blood cells; $QR2_{het}$, QR2 derived from heterologous expression in *E. coli*; NMeH, *N*-methyldihydronicotinamide; RBC, red blood cells.

10.1021/bi035923w CCC: $27.50
Published on Web 03/25/2004

mediate. Thus, QR1 is proposed to function via two half-reactions that make up the overall ping-pong mechanism, namely, direct hydride transfer from NAD(P)H to FAD followed by another direct hydride transfer from $FADH_2$ to quinone. This obligate two-electron mechanism contrasts with many other cellular reductases and allows QR1 to divert quinones from one-electron reductions that could lead to formation of reactive oxygen species and/or depletion of cellular reductants.

Given the high similarity in both primary amino acid sequence and tertiary structure, the mechanism and specificity of QR2 are expected to very similar to QR1. Thus, a similar ping-pong mechanism has been proposed though not shown (*9*), albeit with nonphosphorylated dihydronicotinamides. However, significant differences other than the preference for nicotinamides have been observed. For example, QR2 is not significantly inhibited by dicoumarol (*6*) but is instead potently inhibited by polycyclic aromatic hydrocarbons such as benzo[*a*]pyrene and 1,2-benz[*a*]anthracene, compounds that do not affect QR1 (*13*). These aromatic compounds are competitive with the hydrogen donor NMeH but not with menadione (*14*) and are proposed to bind in the enlarged substrate/nicotinamide cavity created by the absence of a C-terminal tail (*6*). Additionally, the crystal structure of QR2 revealed an unexpected metal binding site that contained zinc in the *Escherichia coli*-expressed form of the enzyme (*9*). However, the metal site, which is completely conserved among all known QR2s, has metal-ion ligands consisting of two histidines, one cysteine, and a main-chain carbonyl, more typical of a type I copper site. This, along with its location on the protein surface, suggests that copper may be involved in the electron-transfer process of QR2, perhaps allowing a one-electron stepwise mechanism that differs significantly from the mechanism for QR1.

We have recently used a functional proteomics approach to purify QR2 from human red blood cells (RBC) that lack QR1 (*15*). Quinacrine, chloroquine, and primaquine, three quinolines that demonstrate antimalarial activity eluted QR2 and aldehyde dehydrogenase specifically from an ATP−Sepharose affinity column loaded with RBC extracts. Additionally, using a primaquine or a chloroquine affinity column, we were able to affinity-purify both QR2 and aldehyde dehydrogenase. We further characterized the selectivity of QR2 for these antimalarials by showing that they inhibit the homologous enzyme QR1 with 1−2 orders of magnitude less potency. This discovery thus presents a novel potential cellular target for these highly successful yet mechanistically poorly understood class of antimalarials. In this paper, we have further characterized the detailed mechanism of inhibition of this class of molecules following a more comprehensive study of the kinetics of the steady-state and single-turnover reductive half-reaction mechanism of QR2.

MATERIALS AND METHODS

Purification of Native and Recombinant QR2 ($QR2_{nat}$ and $QR2_{het}$). $QR2_{nat}$ derived from human RBC was purified using primaquine affinity chromatography as previously described (*15*). To prepare recombinant $QR2_{het}$, human QR2 was PCR-amplified from a human liver cDNA library (Clontech) with the primers: 5′-GCTATGGCAGGTAAGAAAGTACTC-3′ and 5′-GCCACAGAGTTATTGCCCGAAGTG-3′. The amplicon was TA-cloned into pCR2.1 (Invitrogen) and subcloned into a pGEX-4T-2 glutathione-*S*-transferase (GST) expression vector (Amersham Pharmacia). GST-tagged $QR2_{het}$ was transformed and expressed in a BL-21 strain of *E. coli*. GST-tagged $QR2_{het}$ was purified over glutathione Sepharose and released with thrombin cleavage according to the manufacturers instructions (Amersham Pharmacia). Purified $QR2_{nat}$ and $QR2_{het}$ were quantitated by the method of Bradford, and purity was ascertained by SDS−PAGE visualized with silver staining. Purified $QR2_{het}$ and $QR2_{nat}$ were concentrated with Millipore centrifical concentrators and dialyzed against 50 mM Tris−HCl at pH 8.0 at 4 °C before use. The molecular weight of $QR2_{het}$ was determined by gel filtration on a Smart FPLC system (Pharmacia) outfitted with a Superose 12 column (Pharmacia) with a bed volume of 2.4 mL. Molecular weight standards included blue dextran, albumin, ovalbumin, and chymotrypsinogen. Metal-ion determinations were performed by graphite furnace atomic absorption spectrometry with Zeeman background correction at Wake Forest University or by neutron activation analysis at A & L Laboratories, Memphis, TN.

Steady-State Kinetics. Steady-state activity of QR2 was measured on a Hewlett−Packard 8453 multichannel spectrophotometer by monitoring the loss in absorbance of NMeH at 360 nM at 25 °C. Reactions were initiated by the addition of 50−75 pM QR2 to 1 mL of 50 mM Tris at pH 8.5, 0.1% Triton X-100 containing 1.5−40 μM menadione (Sigma), and 4−100 μM NMeH (prepared as described previously, *16*). Reaction rates were converted to specific activity using $\epsilon_{360} = 7060\ M^{-1}\ cm^{-1}$ for NMeH. The enzyme concentration was determined using the Bio-Rad assay. Values plotted are the absolute values of the mean of three independent rate observations calculated from the linear portion of the reaction. Data sets were fitted to standard equations describing steady-state kinetics for substrate binding and competitive and uncompetitive inhibition in order to derive K_m, K_i, K_{ii}, and V_{max} values (*17*). Having observed ping-pong kinetics at low concentrations of both substrates (data not shown) and strong substrate inhibition at higher concentrations of menadione, we fitted our ping-pong kinetics with substrate inhibition to eq 1 where v_{obs} is the observed reaction rate, V

$$v_{obs} = \frac{VAB}{K_a B\left(1 + \frac{B}{K_{iB}}\right) + K_b A + AB} \qquad (1)$$

is the maximum rate, A and B are the concentrations of NMeH and menadione, respectively, K_a and K_b are the Michaelis constants for substrates A and B, and K_{iB} is the competitive binding constant of substrate B. For all graphs, the plotted points represent the observed data, and the best-fit lines are derived from the constants K_m, K_i, K_{ii}, and V_{max} calculated with KinetAsystII. For deriving global fits to eq 1, we followed the precedent for nucleoside diphosphate kinase (*18*). Specifically, by replotting the intercepts from all of the data of 1/[NMeH] versus $1/v_{obs}$ (eight concentrations of menadione versus eight concentrations of NMeH), we derived an apparent V_{max} and an apparent K_m (=9 μM) for menadione. Next, we used the parallel lines in the Lineweaver−Burk plot at low concentrations of menadione to estimate a K_m for NMeH (=5 μM). We used the

Table 1: Simple Michaelis−Menten Values of $QR2_{nat}$ and $QR2_{het}$ at Steady-State Parameters as Measured under the Indicated Reaction Conditions

varied substrate	fixed substrate	$QR2_{het}$ K_m (μM)	$QR2_{het}$ k_{cat} (s^{-1})	$QR2_{nat}$ K_m (μM)	$QR2_{nat}$ k_{cat} (s^{-1})
NMeH	menadione (40 μM)	41 ± 5	215 ± 23	17 ± 4	201 ± 51
menadione	NMeH (100 μM)	4.1 ± 0.9	276 ± 21	3.5 ± 1.0	189 ± 53

intersecting lines in the Lineweaver−Burk plot at high concentrations of menadione to estimate the K_i for menadione (=30 μM). Finally, we applied these estimates to globally fit all of the data simultaneously to eq 1 using weighted least-squares minimization.

Inhibition kinetics with chloroquine, quinacrine, and primaquine versus the substrates menadione and NMeH were determined using the same assay techniques as in the steady-state kinetics above. The reaction mechanism was determined qualitatively by inspection of the double-reciprocal plots, and inhibition constants were calculated by fitting to the standard equations for competitive, uncompetitive, and noncompetitive inhibition using KinetAsystII (*17*). Inhibition models were excluded if the derived constants were excessively large, the errors were large, or the fitting algorithm failed to converge (see Supplemental Table 1 in the Supporting Information).

Pre-Steady-State Kinetics. FAD absorption on the enzyme was monitored under quasi-anaerobic conditions at 450 nm and a 1 cm path length with an Applied Photonics SX.18MV stop-flow instrument. Anaerobic conditions were achieved according to the instrument instructions. Solutions were evacuated overnight and equilibrated in a glovebox with ultrahigh pure nitrogen for at least 2 h prior to use. All reactions contained the specified amount of enzyme and substrate in 50 mM Tris at pH 8.5 and 0.1% Triton X-100 (vol/vol). The stop-flow instrument was thermostated with a circulating water bath at the temperature indicated. Time-course data were fit to either single- (eq 2) or double-phase (eq 3) exponential decay equations using the SX.18MV software. Substrate concentration dependence in single-

$$\text{signal} = \text{Amp}^{(-kt)} + \text{plateau} \quad (2)$$

$$\text{signal} = \text{Amp1}^{(-k_1 t)} + \text{Amp2}^{(-k_2 t)} + \text{plateau} \quad (3)$$

turnover experiments with [E] ≫ [S] was fitted to eq 4 and with [S] > [E] was fitted to eq 5.

$$k_{obs} = k_1[\text{QR2}] + k_{-1} \quad (4)$$

$$k_{obs} = \frac{k_{max}[\text{NMeH}]}{K_d + [\text{NMeH}]} \quad (5)$$

Direct Measurement of Inhibitor Binding to QR2. To measure the binding of the quinolines to specific redox states of QR2 by an independent assay, we monitored the fluorescence signal of the oxidized cofactor in the presence of increasing concentrations of the inhibitors. QR2 (0.8−1.1 μM) was incubated with primaquine or chloroquine (0.5−12 μM) in 50 mM Tris−HCl (pH 8.5) at 25 °C in a Perkin−Elmer LS-50B fluorimeter. The flavin was excited at 450 nm (5 nm slit width), and emission was detected at 515 nm (10 nm slit width). Each point represents the average of five readings. The binding data were fitted to eq 6 where K_d is the dissociation constant, $[QR2]_t$ and $[PQ]_t$ are the total concentrations of enzyme and primaquine in the cuvette, and c is an experimentally determined constant that relates fluorescence intensity to concentration.

$$\Delta F = \{(K_d + [\text{QR2}]_t + [\text{PQ}]_t) - \sqrt{(K_d + [\text{QR2}]_t + [\text{PQ}]_t)^2 - 4[\text{QR2}]_t[\text{PQ}]_t}\}/2c \quad (6)$$

RESULTS

Enzyme Purification, Oligomeric State, and Metal Analysis. QR2 was purified to near homogeneity both from human RBC ($QR2_{nat}$) and from a heterologous *E. coli* expression system ($QR2_{het}$) with typical yields of 4 and 0.5 mg/L, respectively. $QR2_{het}$ and $QR2_{nat}$ were >99% pure based on SDS−PAGE analysis visualized with silver stain (data not shown). The minor contaminants in the enzyme preparation of $QR2_{het}$ are HSP-70 and GST−QR2, as determined by mass spectroscopy (data not shown). Analysis of $QR2_{het}$ by gel filtration indicates that the enzyme is entirely in the dimeric state (data not shown), as previously reported (*6*). Metal-ion content of both $QR2_{het}$ and $QR2_{nat}$ was substoichiometric in both zinc (0.1−0.2 equiv) and copper (0.2−0.3 equiv), as determined by graphite furnace atomic absorption spectrometry with Zeeman background correction and neutron activation analysis.

Steady-State Kinetic Mechanism of $QR2_{het}$ and $QR2_{nat}$. We were interested in determining the basic kinetic mechanism of QR2 and comparing the activity of $QR2_{het}$ to $QR2_{nat}$. The k_{cat}'s and K_m's of $QR2_{het}$ and $QR2_{nat}$ for NMeH determined at 40 μM menadione are very similar, as are the k_{cat}'s and K_m's for menadione determined at 100 μM NMeH (Table 1). These data provided an initial indication that $QR2_{het}$ and $QR2_{nat}$ behave similarly despite their differing sources and methods of preparation. These kinetic parameters are a factor of 2−3-fold higher than the specific activities previously determined in both the initial and rediscovery of the enzyme (*6*, *14*). Addition of exogenous metal ions such as zinc (1 mM) or copper (1 mM) did not affect the activity of either $QR2_{het}$ or $QR2_{nat}$, despite the fact that both enzymes appear to contain only substoichiometric amounts of metal. Additionally, extensive dialysis against EDTA (100 mM) or addition of EDTA (100 mM) into the reaction solution did not significantly alter the activity of the enzyme (data not shown). These data indicate that there is no apparent role for a metal ion using the menadione and NMeH substrates for QR2.

Further experiments aimed at determining the kinetic mechanism of QR2 showed ping-pong kinetics at low concentrations for both of the substrates and potent substrate inhibition at high concentrations of menadione, particularly when the concentrations of NMeH were low. This substrate inhibition was still observed following recrystallization of menadione and confirmation of its purity by NMR and mass spectrometry (data not shown). This suggests that menadione

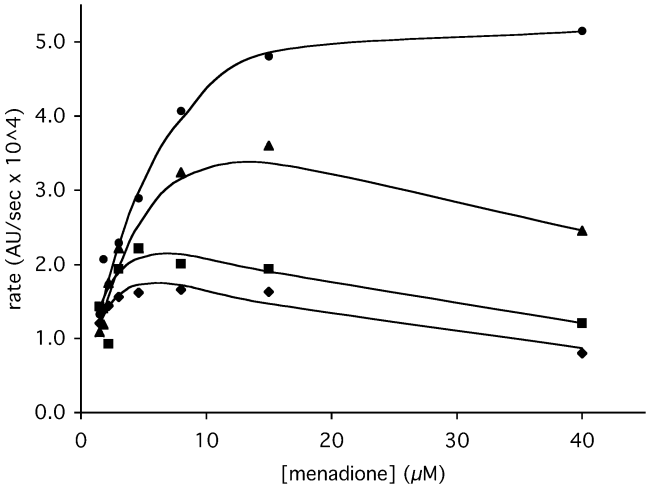

FIGURE 1: Ping-pong kinetics with substrate inhibition. Representative traces from the bisubstrate pattern performed in order to determine the kinetic parameters in Table 2 are shown for $QR2_{het}$. The concentration of menadione was varied as indicated on the *x* axis at the following different concentrations of NMeH: 5 (◆), 9 (■), 25 (▲), and 100 (●) μM. Data points are actual measured rates, and the lines are the best fits derived from the global fitting procedure as described in the Materials and Methods.

Table 2: Steady-State Parameters for $QR2_{nat}$ and $QR2_{het}$ Calculated by Global Fitting to Eq 1 as Described in the Materials and Methods

kinetic parameter	$QR2_{het}$	$QR2_{nat}$
k_{cat} (s^{-1})	462 ± 103	858 ± 227
$K_{m(menadione)}$ (μM)	9.4 ± 3.2	11.6 ± 3.0
$K_{i(menadione)}$ (μM)	13.1 ± 4.7	15.6 ± 8.1
$K_{m(NMeH)}$ (μM)	17.9 ± 3.3	30.3 ± 2.8

itself, and not a contaminant, is the source of the observed inhibition, presumably by binding to the wrong oxidation state of the enzyme. We therefore assumed menadione is competing for NMeH binding in performing and analyzing the kinetics of the expected ping-pong mechanism of QR2 (see the Materials and Methods for details on data fitting). The global fitting to eq 1 describing inhibition of menadione in the NMeH site of a ping-pong mechanism is shown in Figure 1 and Table 2 for both $QR2_{nat}$ and $QR2_{het}$. Thus, QR2, like QR1 (*10*), as predicted previously and visualized in the crystal structure (*9*), has a single substrate binding site alternatively occupied by menadione or NMeH. We note that the apparent K_i for menadione is very similar to its K_m for both $QR2_{nat}$ and $QR2_{het}$. This suggests that the oxidized and reduced forms of the enzyme bind menadione with similar potency, revealing poor discrimination for the correct substrate (NMeH) in the oxidized form of the enzyme. Although $QR2_{nat}$ appears to have a higher k_{cat}, we believe this difference is not significant given the difficulties of fitting kinetics with such potent substrate inhibition. Specifically, minor adjustments within the experimental error (<20%) in the ratios of K_i's and K_m's easily have 2-fold impacts on the global best-fit V_{max}'s.

Stop-Flow Kinetic Analysis of $QR2_{het}$ Reduction by NMeH. With sufficiently large amounts of enzyme available through heterologous expression in *E. coli*, we set out to further investigate the details of the kinetic mechanism of the enzyme. Single-turnover experiments were performed to address whether substrate binding or events on the enzyme (e.g., chemistry) are rate determining for the reductive half-

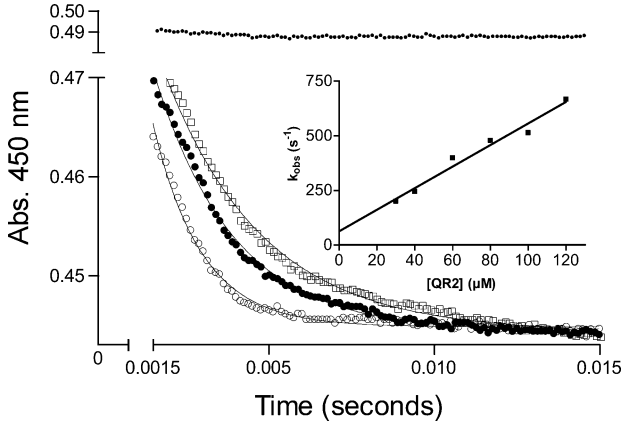

FIGURE 2: Representative single-turnover time courses for the reduction of QR2 monitored by the disappearance of FAD absorbance at 450 nm at 4 °C. Kinetic traces were obtained by mixing 40 (□), 60 (●), and 120 (○) μM QR2 (final concentration) with 3 μM NMeH or 160 μM QR2 with 0 μM NMeH (●). Solid lines represent the fit of the data to a single-exponential decay function (eq 2) to obtain k_{obs}. Only data points later than the dead time of the instrument (1.5 ms) are displayed. Inset: Observed rates (k_{obs}) obtained from the single-exponential fit of the time course plotted as a function of the concentration of QR2. Linear regression of these data yields a slope of (4.36 ± 0.06) × 10^6 M^{-1} s^{-1} and a *y* intercept of 156 ± 5 s^{-1}.

reaction (*19*). QR2−FAD (oxidized form) is yellow and absorbs strongly at 450 nm, while QR2−$FADH_2$ (reduced form) is colorless at this wavelength. Menadione was omitted from the reaction in order to prevent the reoxidation of the enzyme, and therefore, only the rate of the reductive half-reaction was observed. Attempts to monitor the rate of NMeH binding at these high concentrations of $QR2_{het}$ at 25 °C were not possible because the reaction went to completion within the dead time of the instrument (data not shown). Thus, to determine the mechanism and rate of substrate binding, single-enzyme-turnover reactions were monitored by following the rate of enzyme-bound FAD reduction at 4 °C. To ensure pseudo-first-order kinetics, the concentration of $QR2_{het}$ (30, 40, 60, 80, 100, or 120 μM) was at least 10-fold in excess over the substrate (3 μM). Time-course data were fit to a single-phase exponential decay according to eq 2, and representative traces are shown in Figure 2. The amplitudes of the curves are in good agreement with the calculated theoretical changes in amplitude based on an extinction coefficient of 11 300 M^{-1} cm^{-1} for FAD (*20*). Less than a 10-fold enzyme excess required a two-phase exponential decay model to describe the data (data not shown). Replots of the observed rate constant versus the enzyme concentration show the expected linear behavior of rate-determining substrate association (Figure 2, inset). The replotted data were fitted to eq 4 to yield k_{on} and k_{off} rates of (4.9 ± 0.4) × 10^6 M^{-1} s^{-1} and 62 ± 3 s^{-1}, respectively. This generates a calculated K_d ($=k_{off}/k_{on}$) of 12.7 μM, compared to the K_m of 17.9 μM seen in the steady-state kinetics. Using the simplest kinetic model, wherein $K_m = (k_{-1} + k_2)/k_1$, one can calculate an apparent k_2 of 26 ± 20 s^{-1} at 4 °C under these subsaturating concentrations of the substrate (see below). Given the large errors possible in this type of analysis and the differing conditions of enzyme concentrations (5 μM in stopped flow and 50 pM in steady state), this value compares quite favorably with the expected rate constant derived from the steady-state kinetics of >460

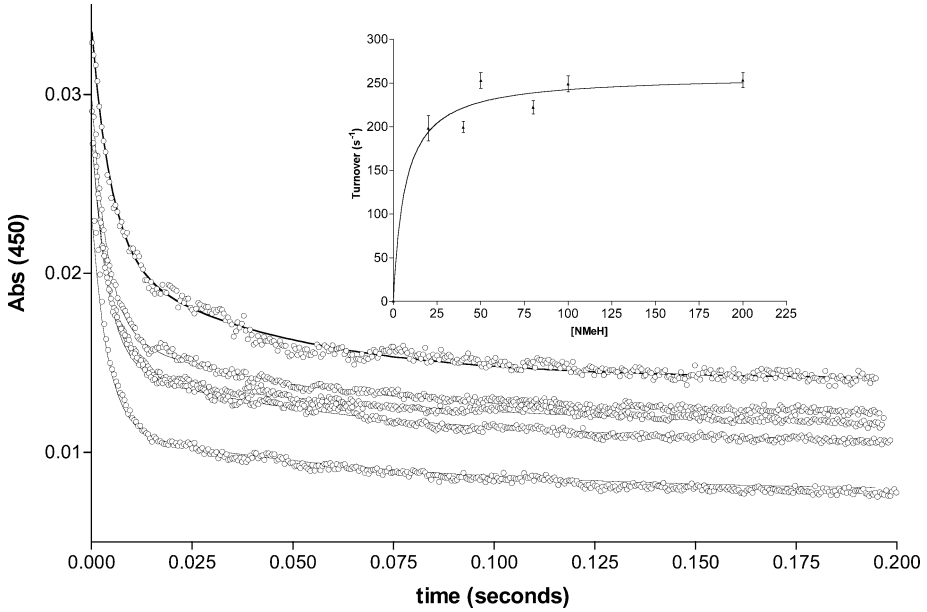

FIGURE 3: Representative single-turnover time courses for the reduction of QR2 monitored by the disappearance of FAD absorbance at 450 nm at 25 °C. Kinetic traces were obtained by mixing 5.5 μM QR2 with 20, 50, 80, 100, or 200 μM NMeH (listed from the bottom to uppermost trace). The data were fitted with a double-phase exponential decay (eq 3). Amp1 of the fast rate constant accounted for 80% of the signal, and Amp2 of the slow rate constant accounted for 20% of the signal. Data points cover the line where it is not visible. Inset: Observed fast constants from the double-exponential fit plotted as a function of the concentration of NMeH. The data were fitted to eq 4 to yield a K_d of 7 ± 3 μM and a k_{max} of 258 ± 15 s^{-1}.

s^{-1} at 25 °C (Table 2) and 98 ± 18 s^{-1} at 4 °C (data not shown). As expected, there was no appreciable difference in the observed rates using twice as much substrate at 60, 70, 80, or 100 μM QR2 (data not shown). Single-turnover kinetics of the oxidative half-reaction using menadione and reduced QR2 could not be performed because of the instability of the reduced enzyme and our inability to achieve sufficiently anaerobic conditions.

We also performed single-turnover analysis of the reductive half-reaction at high concentrations of the substrate NMeH. Although this potentially complicates the model fitting because of the nonlimiting conditions, these reactions can be performed using much less enzyme and much more substrate and therefore occur over a more extended time course with larger spectrophotometric signals. Thus, these experiments at higher substrate concentrations are optimized to detect potential reaction intermediates occurring after substrate binding such as charge-transfer complexes or one-electron reduced states of the enzyme. Stop-flow analysis of the reduction of 5.5 μM $QR2_{het}$ with 20−200 μM NMeH was followed by monitoring the absorbance of enzyme-bound oxidized FAD at 450 nm. Time-course data were fit to monophasic (eq 2, not shown) and biphasic models (eq 3, Figure 3). Visual inspection and error residuals clearly showed that the biphasic curve best describes the data. The fast rate, corresponding to 80% of the observed signal, is shown plotted as a function of substrate concentration in the inset to Figure 3. The fitted K_d of 7 ± 3 μM and k_{max} of 258 ± 15 s^{-1} are in reasonable agreement with the K_d of 12.7 μM determined in the single-turnover conditions and the turnover number of 462 ± 103 s^{-1} determined under steady-state conditions. The apparent saturation at these high concentrations of NMeH indicates that under these conditions substrate association is no longer rate-determining. The slow rate, corresponding to the remaining 20% of the signal, shows no dependence on substrate concentration and an average k_{obs} of 16 ± 4 s^{-1} (data not shown). Note that this slow rate is not kinetically competent to be on the normal reaction path. It is unlikely that this slow rate represents a heterogeneity in the enzyme preparation or of the bound FAD cofactor, for at least two reasons. First, $QR2_{het}$ is highly purified and completely dimeric by size-exclusion chromatography. Additionally, the single-turnover kinetics performed with limiting substrate showed only one phase (Figure 2). (The second phase would be of sufficient magnitude, 0.01 AU, to be observed with the amount of NMeH used in the reaction, 0.05 AU.) We postulate that the observed slow reaction is the result of a rereduction of QR2 that is being slowly oxidized back to the starting form by low concentrations of residual oxygen in the sample. This interpretation is consistent with the difficulty in preparing stable reduced QR2.

The observed saturation of the rapid reaction kinetics at high substrate concentrations suggested that it may be possible to observe an intermediate species formed after enzyme−substrate association. However, we were unable to detect the formation of any intermediate enzyme forms by performing stopped-flow analyses at 10 nm increments from 320 to 620 nm (Figure 4). Specifically, mixing 33.8 μM QR2 with 50 μM NMeH indicated no spectrophometrically unique species, in particular, none with an absorbance greater than 500 nm that would be indicative of a red-shifted semiquinone. The lack of an observable intermediate is consistent with the fitting of the majority of the detected FAD reduction signal to a single exponential (Figure 3). Thus, our reaction kinetics share significant similarity to those of QR1 and are most consistent with a direct hydride transfer from the electron donor to the flavin (*10*, *11*).

Steady-State Inhibition of QR2. To build on our initial observation of inhibition of QR2 by the quinolines (*15*) and further describe the kinetic mechanism of inhibition of QR2 by chloroquine, quinacrine, and primaquine, enzyme activity

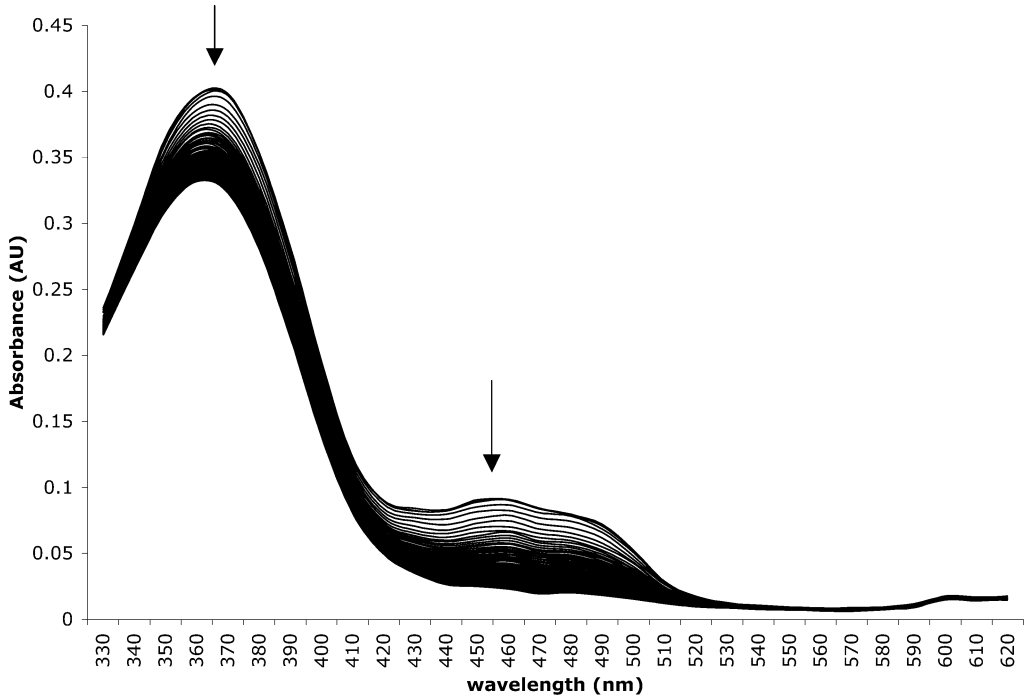

FIGURE 4: Reaction of 33.8 μM QR2 and 50 μM NMeH (final concentrations) monitored by stopped-flow photodiode array spectroscopy every 10 nm from 320 nm to 620 nm. Arrows indicated the change in absorption over the 10 s reaction course.

as a function of both the inhibitor and substrate concentrations was measured. Conditions were chosen to minimize substrate inhibition by menadione to facilitate fitting of the data to the standard equations describing inhibition. Primaquine is a competitive inhibitor of QR2 with respect to the electron donor NMeH and an uncompetitive inhibitor of QR2 with respect to menadione (parts A and B of Figure 5; Supplemental Tables 1A and 1B in the Supporting Information). In contrast to primaquine, quinacrine and chloroquine were competitive inhibitors of QR2 with respect to menadione (parts D and F of Figure 5; Supplemental Tables 1D and 1F in the Supporting Information) and uncompetitive inhibitors with respect to NMeH (parts C and E of Figure 5; Supplemental Tables 1C and 1E in the Supporting Information). The inhibition constants (K_i and K_{ii}) ranged from 220 nM to 2 μM (Table 3). Collectively, these data suggest that the quinoline drugs bind QR2 in the single cofactor/substrate binding pocket inferred from the ping-pong kinetics described above and the previously determined crystal structure (*9*). Interestingly, although these compounds have only subtle structural differences (Figure 8), they show a surprising discrimination for the different oxidation states of the enzyme (see the Discussion).

Pre-Steady-State Inhibition of QR2. To further verify the ability of the quinolines to inhibit a specific redox state of QR2, pre-steady-state reaction kinetics of the enzyme were investigated. The rate of QR2 reduction was followed as above following rapid mixing of equal volumes of oxidized QR2 and NMeH in the presence or absence of a saturating concentration of a quinoline drug (100 $\times$ K_i). As seen in Figure 6, 100 μM primaquine strongly inhibited FAD reduction, while 60 μM chloroquine showed essentially no inhibition. Nonlinear regression analysis of the data confirms the visually dramatic results, with no significant changes in the fitting parameters required for the chloroquine data (not shown). The small signal for the primaquine data precluded comparative fitting of the data. Thus, these data confirm that primaquine is a potent inhibitor of FAD reduction, while chloroquine inhibition of this form of the enzyme is modest.

Direct Measurement of Inhibitor Binding to QR2. To confirm the binding of the quinolines to specific redox states of QR2 by an independent assay, we hypothesized that the aromatic rings of the inhibitors could interact with the FAD ring in a manner analogous to the binding of menadione to QR2 seen in the crystal structure. We thus monitored the fluorescence signal of the oxidized cofactor in the presence of increasing concentrations of the inhibitors. As seen in Figure 7, primaquine, but not chloroquine, showed a saturation plot indicative of binding that could be fitted to a K_d of 1.0 ± 0.2 μM, in good agreement with the value determined from the steady-state kinetics ($K_i = 1.0 \pm 0.4$ μM).

DISCUSSION

We have recently proposed that QR2 may be a cellular target for the highly successful yet mechanistically less well understood antimalarial quinoline compounds (*15*). To investigate our hypothesis further, we have undertaken a more detailed kinetic study of QR2 in terms of its mechanism and its interaction with the quinoline compounds. As a goal for these studies, we would like to address the physiological context of inhibition, which is admittedly hampered by the lack of knowledge of the true physiological substrates for QR2. However, validating the use of $QR2_{het}$, deriving the mechanism of inhibition, and determining true binding constants are essential steps along this path. These results will allow for the design of improved inhibitors to further test our hypothesis and the physiological role of QR2.

By comparing $QR2_{het}$ to $QR2_{nat}$, we have shown that the heterologously produced enzyme is a useful and valid tool for investigating the activity of QR2. This is of particular interest because of any putative role for a copper ion in the

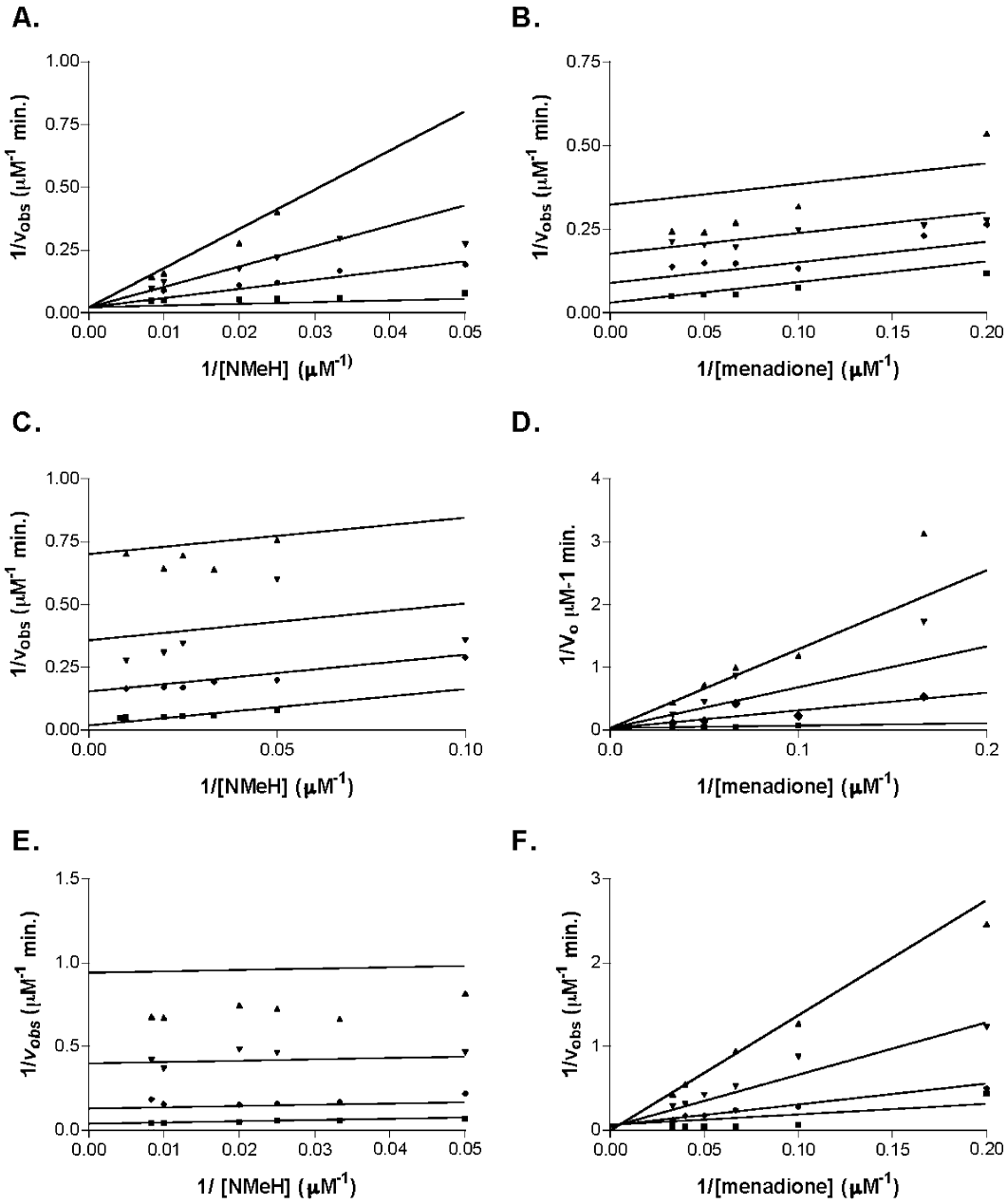

FIGURE 5: Steady-state inhibition of QR2 by quinoline compounds as a function of the substrate concentration. Data in panels A, C, and E have 15 μM menadione and indicated concentration of NMeH, and panels B, D, and F have 60 μM NMeH and indicated concentrations of menadione. Lineweaver−Burk plot of QR2 activity with (A, B) 0 (■), 4 (◆), 10 (▼), and 20 μM (▲) primaquine; (C, D) 0 (■), 4 (◆), 10 (▼), and 20 μM (▲) chloroquine; and (E, F) 0 (■), 0.5 (◆), 2 (▼), and 5 μM (▲) quinacrine. Data points are the mean of three replicates. Solid lines represent best-fit lines calculated according to Cleland's equations using KinetAsystII.

Table 3: Steady-State Inhibition Parameters of Quinoline Compounds for $QR2_{het}$

inhibitor	substrate	type of inhibition	K_i (μM)	K_{ii} (μM)	V (μM/min)	K_m (μM)
chloroquine	NMeH	uncompetitive		1.1 ± 0.2	26 ± 6	23 ± 11
	menadione	competitive	0.6 ± 0.1		27 ± 2	10 ± 2
primaquine	NMeH	competitive	1.0 ± 0.4		22 ± 2	13 ± 6
	menadione	uncompetitive		2.0 ± 0.3	28 ± 3	11 ± 3
quinacrine	NMeH	uncompetitive		0.22 ± 0.05	26 ± 5	20 ± 12
	menadione	competitive	0.51 ± 0.17		15 ± 4	18 ± 10

catalytic cycle, as suggested by the potentially adventitious zinc ion observed in the crystal structure of QR2 (*9*). The lack of any role for a metal ion in catalysis is further supported by our observation of substoichiometric levels of zinc and copper in both $QR2_{het}$ and $QR2_{nat}$ and the lack of any effects by addition of exogenous EDTA, copper, or zinc. Thus, a direct hydride transfer, as reinforced by the proximal location of menadione to the FAD cofactor in the crystal structure, is the most likely chemical mechanism for QR2.

The crystal structure of QR2 suggests that there is only one substrate binding site, alternatively occupied by the reductant or the quinone substrate. This hypothesis is

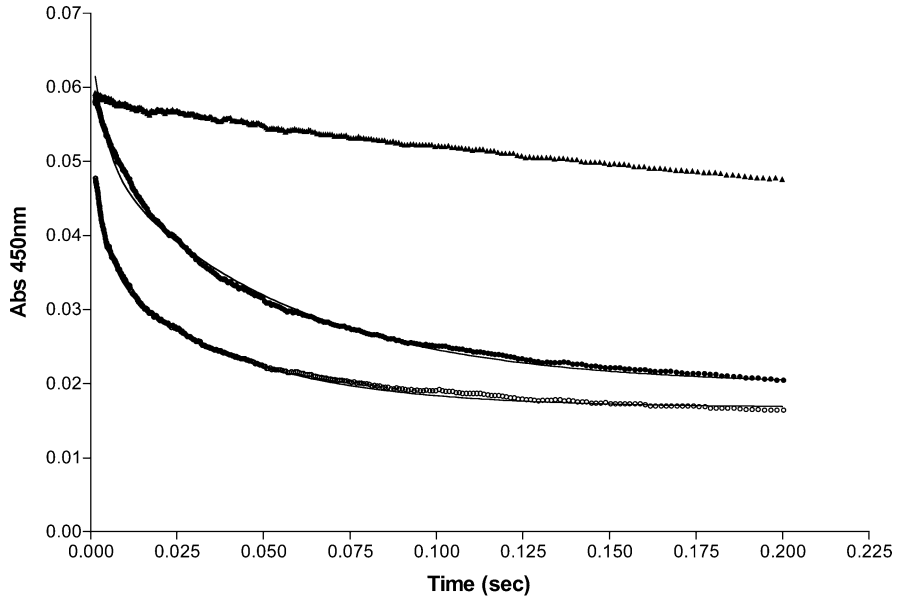

FIGURE 6: Pre-steady-state kinetic traces of the time course of QR2 inhibition by saturating concentrations of primaquine or chloroquine as monitored by FAD reduction. A total of 5.5 μM QR2 was mixed with 10 μM NMeH (○), 10 μM NMeH + 100 μM primaquine (▲), or 10 μM NMeH + 60 μM chloroquine (●). Control and chloroquine data were fitted to a two-phase exponential decay model (eq 3). The line is within the data symbols where it is not visible. The data with primaquine were not fitted.

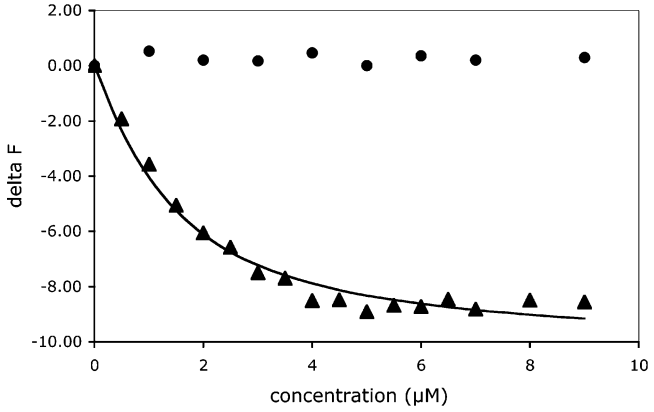

FIGURE 7: Direct measurement of primaquine binding to oxidized QR2 as monitored by FAD fluroescence. A total of 0.89 μM QR2 was mixed with increasing concentrations of primaquine (▲) or chloroquine (●). Data were fitted to eq 6.

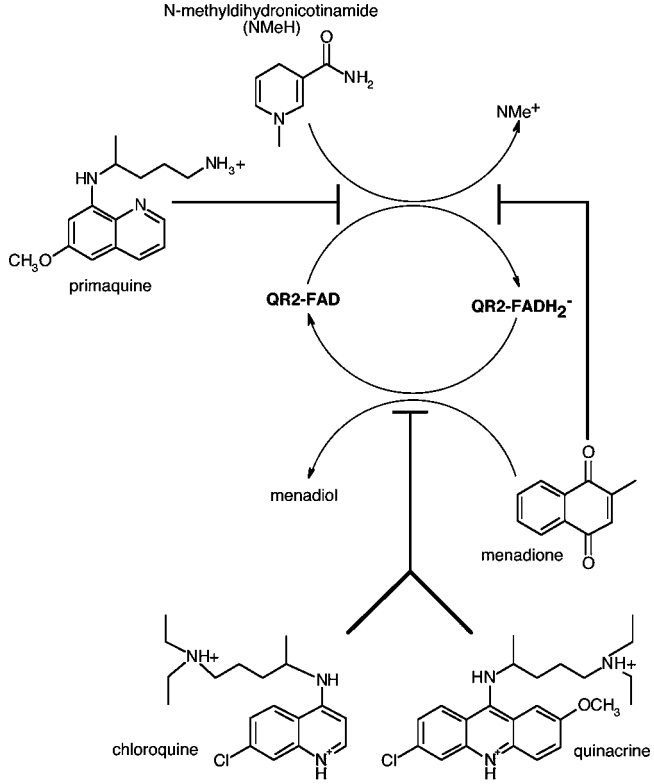

FIGURE 8: Bi-bi ping-pong catalytic mechanism of QR2. Structures and mechanisms of primaquine, chloroquine, and quinacrine inhibition are indicated. QR2−FAD represents the oxidized stable form of the enzyme, and QR2−$FADH_2$, the reduced form.

supported by our demonstration of ping-pong kinetics for the substrates NMeH and menadione (Figure 1). This model also suggests that inhibitors will bind at this one site, which is borne out by the observed competitive and uncompetitive inhibition kinetics (Figure 5). Interestingly, our kinetic and binding data demonstrate that there exists discrimination for the different oxidation states of the enzyme, despite the similarities in the structures of the inhibitors (Figure 8). That is, the oxidized form of QR2 binds the correct substrate NMeH, the wrong substrate menadione, and the inhibitor primaquine. Menadione binding to this oxidized and more stable form of the enzyme with essentially identical inhibitory binding (K_i) and Michaelis (K_m) constants is consistent with the observed crystal structure with bound menadione. It has been previously shown that compounds such as benzo[*a*]-pyrene and 1,2-benz[*a*]anthracene also bind to this form of QR2 (*14*). On the other hand, the reduced form of the enzyme binds the correct substrate menadione and the inhibitors chloroquine and quinacrine but not NMeH. This discrimination by certain compounds for different oxidation states is curious given that the menadione in the crystal structure makes no direct contacts to the protein, instead lying directly on top of the FAD cofactor. Additionally, on the basis of other FAD-containing enzymes, we expect that there is little change in conformation upon oxidation/reduction of FAD (*21*−*23*).

We thus hypothesize that this discrimination toward inhibitors is based mainly on the relative charges of the FAD

cofactor and the inhibitor. At neutral pH, oxidized FAD has no net charge and reduced FAD has one negative charge (*24*). Although the ionization state of FAD on QR2 is unknown, all flavoproteins studied so far (with the exception of the riboflavin proteins) have been shown by NMR to bind the reduced cofactor in the anionic form (*25*−*27*). The primary and tertiary amines of the side chains of primaquine, chloroquine, and quinacrine are all protonated and do not provide a source for differentiation. Greater relevance is the heterocyclic nitrogen and its relative location to the amine modification. On the basis of the model compound 4-aminoquinoline, the pK_a of the heterocyclic nitrogen of quinacrine and chloroquine is predicted to be >9.1 (*28*)[2]. On the basis of the model compound 8-aminoquinoline, the pK_a of the heterocyclic nitrogen in primaquine is predicted to be 4.0 (*28*). This dramatic difference in predicted pK_a's is consistent with the calculation of the charge densities on the heterocyclic nitrogens using Hückel molecular orbital theory (*29*). Therefore, at neutral pH, doubly protonated chloroquine and quinacrine bind to the negatively charged reduced cofactor ($FADH_2$), whereas the singly charged primaquine binds to the neutral oxidized cofactor (FAD). This explanation, however, does not account for the promiscuity of the neutral menadione. Ultimately, cocrystallization of QR2 with different bound quinolines may be very informative in understanding this selectivity, although potentially difficult to achieve for quinacrine and chloroquine given the instability of the reduced form of the enzyme.

The selectivity for the oxidation state of the enzyme has an important consequence for the drug discovery process. Although the dissociation constant of an inhibitor (K_i) is intrinsic to the inhibitor, the identity and concentration of the cofactor and substrate directly influence the degree of enzyme inhibition as measured by IC_{50} experiments. This phenomenon can be quantified by the equation relating IC_{50} to the Michaelis constants (K_a and K_b) for a ping-pong reaction mechanism (derived in *30*)

$$IC_{50} = K_i\left[1 + \frac{A}{K_a}\left(1 + \frac{K_b}{B}\right)\right] \quad (7)$$

where A is the concentration of the electron donor and B is the concentration of the quinone substrate. Thus, the actual IC_{50} may be higher or lower than the experimentally determined value, depending on the assay conditions. These issues go beyond the practical concerns involved from the drug discovery point of view. The validity of QR2 as a target of the quinoline antimalarial compounds has been questioned because of the discrepancy between the concentration of drug required to kill parasites in vivo, 0.01−0.05 μM, and the concentration of drug required to inhibit QR2 activity in vitro, 0.2−2 μM. However, as derived in eq 7, the degree of inhibition of a ping-pong enzyme is a function of both the substrate and the cofactor used in the assay, and the endogenous cofactor and substrates of QR2 in vivo are not known. Thus, the possibility that QR2 is an in vivo target of the quinoline drugs should not be excluded based on this discrepancy.

[2] The 6-methoxy or 6-chloro substituents are not expected to significantly perturb the π-electron structure or the pK_a's of these derivatives.

The discrimination by QR2 inhibitors for different oxidation states may also have physiological relevance. Primaquine, for example, is known to have much better efficacy for the liver stages of malarial infection (*31*). Is it possible that the observed selectivity of primaquine for the oxidized form of the enzyme is reflective of the QR2 in liver being more highly oxidized than that in RBC, a much more reducing environment? It seems that the study of QR2 inhibitors, either for purposes of understanding the physiological role of QR2 or as potential antimalarial agents, should take into account this redox-specific selectivity.

In conclusion, our recent paper has demonstrated that QR2 is present in human RBC and that the quinolines can inhibit QR2 activity. How might QR2 participate in the maintenance of the redox status of RBC? Quinones that are physiological substrates of QR2 may contribute to oxidative stress in RBC by at least three mechanisms. These include depletion of glutathione by direct oxidation (*32*), generation of methemoglobin by direct oxidation of oxyhemoglobin (*33*), and formation of semiquinones that auto-oxidize and form reactive oxygen species such as superoxide (*34*). Furthermore, because RBC lack QR1, QR2 is the only enzyme in RBC that can convert quinones directly into hydroquinones (*35*). Therefore, we postulate that QR2 prevents oxidative stress in RBC by reducing the intracellular concentration of quinones and decreasing the concentration of semiquinones and their subsequent contributions to the generation of reactive oxygen species. Thus, quinoline inhibition of QR2 may affect the redox state of erythrocytes through any combination of the following mechanisms: QR2 inhibition may cause an accumulation of quinones and subsequent quinone-derived oxidative stress as described above, or QR2 inhibition could impair the ability of the RBC to deal with excess oxidative stress, which would occur during the colonization of an erythrocyte with *Plasmodium* parasites (*36*). Experiments investigating this hypothesis in QR2-deficient RBC are currently under investigation.

ACKNOWLEDGMENT

We thank Brad Jones in the Chemistry Department at Wake Forest University for metal analysis and Rupa Ray for the cloning of human QR2.

SUPPORTING INFORMATION AVAILABLE

Comparison of steady-state inhibition parameters of QR2 as determined using KinetAsystII. This material is available free of charge via the Internet at http://pubs.acs.org.

REFERENCES

1. Liao, S., and Williams-Ashman, H. G. (1961) Enzymatic oxidation of some non-phosphorylated derivatives of dihydronicotinamide, *Biochem. Biophys. Res. Commun. 4*, 208−213.
2. Ernster, L., and Navazio, F. (1958) Soluble diaphorase in animal tissue, *Acta Chem. Scand. 12*, 595.
3. Benson, A. M., Hunkeler, M. J., and Talalay, P. (1980) Increase of NAD(P)H: quinone reductase by dietary antioxidants: possible role in protection against carcinogenesis and toxicity, *Proc. Natl. Acad. Sci. U.S.A. 77*, 5216−5220.
4. Talalay, P. (1989) Mechanisms of induction of enzymes that protect against chemical carcinogenesis, *Adv. Enzyme Regul. 28*, 237−250.
5. Talalay, P., Fahey, J. W., Holtzclaw, W. D., Prestera, T., and Zhang, Y. (1995) Chemoprotection against cancer by phase 2 enzyme induction, *Toxicol. Lett. 82/83*, 173−179.

6. Zhao, Q., Yang, X. L., Holtzclaw, W. D., and Talalay, P. (1997) Unexpected genetic and structural relationships of a long-forgotten flavoenzyme to NAD(P)H: quinone reductase (DT-diaphorase), *Proc. Natl. Acad. Sci. U.S.A. 94*, 1669−1674.
7. Jaiswal, A. K., Burnett, P., Adesnik, M., and McBride, O. W. (1990) Nucleotide and deduced amino acid sequence of a human cDNA (NQO2) corresponding to a second member of the NAD-(P)H: quinone oxidoreductase gene family. Extensive polymorphism at the NQO2 gene locus on chromosome 6, *Biochemistry 29*, 1899−1906.
8. Li, R., Bianchet, M. A., Talalay, P., and Amzel, L. M. (1995) The three-dimensional structure of NAD(P)H: quinone reductase, a flavoprotein involved in cancer chemoprotection and chemotherapy: mechanism of the two-electron reduction, *Proc. Natl. Acad. Sci. U.S.A. 92*, 8846−8850.
9. Foster, C. E., Bianchet, M. A., Talalay, P., Zhao, Q., and Amzel, L. M. (1999) Crystal structure of human quinone reductase type 2, a metalloflavoprotein, *Biochemistry 38*, 9881−9886.
10. Tedeschi, G., Chen, S., and Massey, V. (1995) DT-diaphorase. Redox potential, steady-state, and rapid reaction studies, *J. Biol. Chem. 270*, 1198−1204.
11. Tedeschi, G., Chen, S., and Massey, V. (1995) Active site studies of DT-diaphorase employing artificial flavins, *J. Biol. Chem. 270*, 2512−2516.
12. Prochaska, H. L., and Talalay, P. (1986) Purification and characterization of two isofunctional forms of NAD(P)H: quinone reductase from mouse liver, *J. Biol. Chem. 261*, 1372−1378.
13. Liao, S., and Williams-Ashman, H. G. (1961) Inhibition of enzymic oxidation of some dihydropyridines by polycyclic aromatic hydrocarbons, *Biochem. Pharmacol. 6*, 53−54.
14. Liao, S., Dulaney, J. T., and Williams-Ashman, H. G. (1962) Purification and properties of a flavoprotein catalyzing the oxidation of reduced ribosyl nicotinamide, *J. Biol. Chem. 237*, 2981−2987.
15. Graves, P. R., Kwiek, J. J., Fadden, P., Ray, R., Hardeman, K., Coley, A. M., Foley, M., and Haystead, T. A. (2002) Discovery of novel targets of quinoline drugs in the human purine binding proteome, *Mol. Pharmacol. 62*, 1364−1372.
16. Ortiz-Maldonado, M., Gatti, D., Ballou, D. P., and Massey, V. (1999) Structure−function correlations of the reaction of reduced nicotinamide analogues with p-hydroxybenzoate hydroxylase substituted with a series of 8-substituted flavins, *Biochemistry 38*, 16636−47.
17. Cleland, W. W. (1979) Statistical analysis of enzyme kinetic data, *Methods Enzymol. 63*, 103−38.
18. Garces, E., and Cleland, W. W. (1968) Kinetic studies of yeast nucleoside diphosphate kinase, *Biochemistry 8*, 633−640.
19. Johnson, K. (1992) Transient-state kinetic analysis of enzyme reaction pathways, *Enzymes 20*, 1−61.
20. Ghisla, S., Massey, V., Lhoste, J. M., and Mayhew, S. G. (1974) Fluorescence and optical characteristics of reduced flavines and flavoproteins, *Biochemistry 13*, 589−597.
21. Binda, C., Angelini, R., Federico, R., Ascenzi, P., and Mattevi, A. (2001) Structural bases for inhibitor binding and catalysis in polyamine xxidase, *Biochemistry 40*, 2766−2776.
22. Ludwig, M. L., Pattridge, K. A., Metzger, A. L., and Dixon, M. M. (1996) Control of oxidation−reduction potentials in flavodoxin from Clostridium beijerinckii: The role of conformation changes, *Biochemistry 36*, 1259−1280.
23. Picaud, T., and Desbois, A. (2002) Electrostatic control of the isoalloxazine environment in the two-electron reduced states of yeast glutathione reductase, *J. Biol. Chem. 277*, 31715−31721.
24. Bruice, T. C. (1976) Models and flavin catalysis, in Progress in Bioorganic Chemistry (Kaiser, E. T., Ed.) Vol. 4, pp 1−87, Wiley & Sons: New York.
25. Muller, F. (1991) Nuclear magnetic resonance studies on flavoproteins, in *Chemistry and Biochemistry of Flavoenzymes* (Muller, F., Ed.) pp 557−595, CRC Press, Boca Raton, FL.
26. Lennon, B. W., Williams, C. H. J., and Ludwig, M. L. (1999) Crystal structure of reduced thioredoxin reductase from *Escherichia coli*: structural flexibility in the isoalloxazine ring of the flavin adenine dinucleotide cofactor, *Protein Sci. 8*, 2366−2379.
27. Fleischmann, G., Lederer, F., Muller, F., Bacher, A., and Ruterjans, H. (2000) Flavin-protein interactions in flavocytochrome b2 as studied by NMR after reconstitution of the enzyme with 13C- and 15N-labelled flavin, *Eur. J. Biochem. 267*, 5156−5167.
28. Dean, J. A. (1985), Lange's Handbook of Chemistry, McGraw−Hill Book Company, New York.
29. Singer, J. A., and Purcell, W. P. (1967) Hückel molecular orbital calculations for some antimalarial drugs and related compounds, *J. Med. Chem. 10*, 754−762.
30. Preusch, P. C., Siegel, D., Gibson, N. W., and Ross, D. (1991) A note on the inhibition of DT-diaphorase by dicoumarol, *Free Radical Biol. Med. 11*, 77−80.
31. Shanks, G. D., Kain, K. C., and Keystone, J. S. (2001) Malaria chemoprophylaxis in the age of drug resistance. II. Drugs that may be available in the future, *Clin. Infect. Dis. 33*, 381−385.
32. Gant, T. W., Doherty, M. D., Odowole, D., Sales, K. D., and Cohen, G. M. (1986) Semiquinone anion radicals formed by the reaction of quinone with glutathione or amino acids, *FEBS Lett. 201*, 296−300.
33. Munday, R., Fowke, E. A., Smith, B. L., and Munday, C. M. (1994) Comparative toxicity of alkyl-1,4-Naphthoquinones in rats: Relatioship to free radical production in vitro, *Free Radical Biol. Med. 16*, 725−731.
34. O'Brien, P. J. (1991) Molecular mechanisms of quinone cytotoxicity, *Chem.-Biol. Interact. 80*, 1−41.
35. Benatii, U., Guida, L., De Flora, A., and Hochstein, P. (1987) The effect of encapsulated DT diaphorase on the sensitivity of human red blood cells to menadione, *Chem. Scr. 27A*, 169−171.
36. Hunt, N. H., and Stocker, R. (1990) Oxidative stress and the redox status of malaria-infected erythrocytes, *Blood Cells 16*, 499−526.

BI035923W